SCIENCE CHINA
Earth Sciences

•RESEARCH PAPER•

September 2018 Vol.61 No.9: 1306–1315
https://doi.org/10.1007/s11430-017-9210-0

Simulated effect of sunshade solar geoengineering on the global carbon cycle

Jiu JIANG, Han ZHANG & Long CAO*

Department of Atmospheric Sciences, School of Earth Sciences, Zhejiang University, Hangzhou 310027, China

Received August 25, 2017; revised December 19, 2017; accepted May 22, 2018; published online June 15, 2018

Abstract Solar geoengineering has been proposed as a potential mechanism to counteract global warming. Here we use the University of Victoria Earth System Model (UVic) to simulate the effect of idealized sunshade geoengineering on the global carbon cycle. We conduct two simulations. The first is the A2 simulation, where the model is driven by prescribed emission scenario based on the SRES A2 CO_2 emission pathway. The second is the solar geoengineering simulation in which the model is driven by the A2 CO_2 emission scenario combined with sunshade solar geoengineering. In the model, solar geoengineering is represented by a spatially uniform reduction in solar insolation that is implemented at year 2020 to offset CO_2-induced global mean surface temperature change. Our results show that solar geoengineering increases global carbon uptake relative to A2, in particular CO_2 uptake by the terrestrial biosphere. The increase in land carbon uptake is mainly associated with increased net primary production (NPP) in the tropics in the geoengineering simulation, which prevents excess warming in tropics. By year 2100, solar geoengineering decreases A2-simulated atmospheric CO_2 by 110 ppm (12%) and causes a 60% (251 Pg C) increase in land carbon accumulation compared to A2. Solar geoengineering also prevents the reduction in ocean oxygen concentration caused by increased ocean temperatures and decreased ocean ventilation, but reduces global ocean NPP. Our results suggest that to fully access the climate effect of solar geoengineering, the response of the global carbon cycle should be taken into account.

Keywords Solar geoengineering, Carbon cycle, Climate change, Ocean biogeochemistry

Citation: Jiang J, Zhang H, Cao L. 2018. Simulated effect of sunshade solar geoengineering on the global carbon cycle. Science China Earth Sciences, 61: 1306–1315, https://doi.org/10.1007/s11430-017-9210-0

1. Introduction

Since the beginning of the industrial revolution, atmospheric CO_2 concentration has increased by 40% primarily as a result of the fossil fuel combustion and human-induced land use change (Ciais et al., 2013). Increasing atmospheric CO_2 traps long-wave radiation, warming the Earth surface and causing climate change (Trenberth et al., 2009). Many studies have investigated the impacts of human activities on climate system and global carbon cycle during the past decades, and demonstrated that anthropogenic CO_2 emissions have important effects on the climate system (Ciais et al., 2013).

Reducing CO_2 emissions is the safest way to prevent undesired effects of anthropogenic climate change, but the reduction in CO_2 emissions is challenging for economic, political, and social reasons (The Royal Society, 2009; Victor et al., 2014). With increasing CO_2 content in the atmosphere, geoengineering has been proposed as a potential means to mitigate climate change resulting from anthropogenic greenhouse gases emissions (Keith, 2000; Crutzen, 2006; Vaughan and Lenton, 2011; Caldeira et al., 2013; National Research Council, 2015a, 2015b).

Geoengineering, also termed as climate engineering, is defined as the large-scale management and alteration applied to the Earth climate system to counteract anthropogenic climate change (Keith, 2000). Geoengineering is usually

* Corresponding author (email: longcao@zju.edu.cn)

divided into two categories: carbon dioxide removal (CDR) and solar radiation management (SRM) (Keith, 2000; The Royal Society, 2009). CDR methods mitigate climate change by intentionally removing anthropogenic CO_2 in the atmosphere (The Royal Society, 2009). SRM methods, also termed as solar geoengineering, reduce incoming solar radiation reaching the Earth surface (The Royal Society, 2009), including space mirror sunshading (Early, 1989), stratospheric aerosol injection (Rasch et al., 2008; Robock, 2014), marine clouds brightening (Salter et al., 2008), and ocean and land albedo modification (Ridgwell et al., 2009).

Numerous studies using different climate models have investigated the climate effects of solar geoengineering. Prior modeling studies on SRM have been conducted with prescribed atmospheric CO_2 concentration (e.g., Govindasamy et al., 2002; Niemeier et al., 2013; Tilmes et al., 2013; Keller et al., 2014; Kalidindi et al., 2015), and thus neglect interactions between SRM and the carbon cycle. To better understand the climate response to solar geoengineering, the Geoengineering Model Intercomparison Project (GeoMIP) synthesizes twelve climate models have been conducted (Kravitz et al., 2011, 2013, 2015). All of these GeoMIP experiments were conducted under prescribed atmospheric CO_2 concentrations and neglected carbon cycle responses.

Here we use an Earth system climate model of intermediate complexity (EMIC) to investigate the effect of SRM on the global carbon cycle and ocean biogeochemistry. Different types of EMIC models have been used to study geoengineering climate effects. For example, Eliseev et al. (2010) used an EMIC model to investigate the dependence of global cooling on the amount and horizontal distribution of sulfate aerosol emission. Brovkin et al. (2009) used an EMIC model to examine the climate response to the termination of sulfate aerosol geoengineering. In this study, we use the UVic EMIC model to examine responses of global carbon cycle and ocean biogeochemistry to solar geoengineering. UVic model is a well-established climate-carbon cycle model that is suitable for studying the interactions between climate change and the carbon cycle over time scales of decades to hundreds of years and longer. Matthews and Caldeira (2007) examined the response of temperature, precipitation, and atmospheric CO_2 to solar geoengineering. Building upon previous studies, our goal here is to investigate in detail the response of both terrestrial and marine carbon cycles to solar geoengineering in the context of interactive carbon cycle feedbacks.

As a first step to understand the effect of solar geoengineering on the global carbon cycle, we use a highly idealized SRM scenario, in which a spatially uniform reduction in incoming solar radiation at the top of atmosphere is imposed in the model. This type of solar geoengineering experiment has been widely applied to modeling studies that investigate climate change in response to sunshade solar geoengineering (Lunt et al., 2008; Irvine et al., 2009; Curry et al., 2014; Cao et al., 2016).

2. Method

2.1 Model description

The model used here is the version 2.9 of the University of Victoria Earth System Climate Model (UVic), which is an Earth system model of intermediate complexity with a prognostic global carbon cycle (Weaver et al., 2001; Schmittner et al., 2008; Eby et al., 2009). The oceanic component is represented by a three-dimension ocean general circulation model with nineteen layers in the vertical, which is coupled to a dynamic/thermodynamic sea-ice model and one layer simple energy-moisture balance atmosphere model. Both the atmosphere and the ocean models have a horizontal resolution of 1.8° latitude by 3.6° longitude. The marine carbon cycle is simulated with an organic carbon cycle that is represented by a simplified Nutrient-Phytoplankton-Zooplankton-Detritus (NPZD) ocean ecosystem model and inorganic carbon cycle that simulates air-sea CO_2 exchange and carbonate chemistry based on the Ocean Carbon-Cycle Model Intercomparison Project (OCMIP, Orr et al., 1999) protocol.

The UVic model also includes a land vegetation and terrestrial carbon cycle model derived from MOSES2 (the land surface model) and TRIFFID (the dynamic vegetation model) of the Hadley Centre (Meissner et al., 2003). The land module also has a horizontal resolution of 1.8° latitude by 3.6° longitude. By coupling the global carbon cycle and physical climate modules, the UVic model can be used as an appropriate tool to study the interactions between the global carbon cycle and climatic changes, as shown in earlier studies (Schmittner et al., 2008; Keller et al., 2014).

2.2 Simulated experiments

To obtain a quasi-equilibrium preindustrial climate system state, the model is spun up for 10000 model years with a constant preindustrial atmospheric CO_2 concentration of 280 ppm. Averaged over the last 100 years, the globally integrated air-sea and air-land CO_2 flux is 0.0±0.02 Pg C (1 Pg C=10^{15} g C) and 0.0±0.06 Pg C (one standard deviation), soil carbon storage is 1231±0.5 Pg C, and the global mean surface temperature is 13.18±0.02°C (Appendix Figure A1, http://link.springer.com), indicating that a quasi-equilibrium state has been reached for both the carbon cycle and climate.

The quasi-equilibrium model state is then used as the initial condition for the subsequent simulated experiments. We used a prescribed time series of CO_2 emissions to drive the model. Between year 1800 and 2015, the time series of CO_2

emissions (Figure 1a) are based on the historical emissions from fossil fuel burning and land use change (Houghton et al., 2012; Boden et al., 2016). From year 2016 to 2100, prescribed emissions are based on IPCC emissions scenario SRES (Special Report on Emissions Scenarios) A2, which represents globally high population growth and intensive fossil fuel combustion in the future (IPCC, 2007). After year 2100, CO_2 emission is assumed to decrease linearly at a rate of 0.13 Pg C per year. By year 2300, CO_2 emission is reduced to zero with a cumulative emission of 5000 Pg C after year 2000. The release of 5000 Pg C fossil fuel is a conservative estimate of fossil fuel resources (IPCC, 2001; Kvenvolden, 2002), and we use this rough estimate to illustrate a future word with long-term intensive CO_2 emissions.

Here we represent solar geoengineering in the model simply by reducing the amount of solar irradiance at the top of atmosphere to mimic the effect of sunshade geoengineering (Matthews and Caldeira, 2007). We model the highly idealized case where the reduction in solar irradiance is assumed to offset radiative forcing from anthropogenic CO_2, which maintains a near-zero global mean surface temperature change in the solar geoengineering simulation. Using the idealized solar geoengineering scenario as an illustration, our focus here is to investigate interactions between climate change and the carbon cycle under solar geoengineering.

Two transient simulations are performed in our study: (1) a simulation under the prescribed A2 emission scenario, termed as A2; (2) a solar geoengineering simulation with the same A2 emission scenario but at the same time the sunshade geoengineering scheme is implemented from year 2020 to 2300, termed as GEO.

The solar geoengineering implementation in the model is simply represented by a reduction in incoming solar radiation, which is calculated following the method of Matthews and Caldeira (2007). In the UVic model, radiative forcing caused by excess atmospheric CO_2 is calculated as the natural logarithm of simulated CO_2 concentrations relative to a preindustrial CO_2 concentration level (Weaver et al., 2001). The amount of required reduction in solar irradiance to offset CO_2-induced radiative forcing is calculated according to

$$K_g S_T\left(1-\alpha_p\right)=F\ln\frac{CO_2}{280.0}. \quad (1)$$

The right-hand side of eq. (1) represents radiative forcing caused by increasing atmospheric CO_2. The left-hand side of eq. (1) represents the amount of solar forcing needed to offset CO_2 forcing. F has constant value of 5.35 W m^{-2}. S_T denotes the incoming solar radiation at each model grid point; α_p denotes the planetary albedo at each model grid, which is calculated as reflected solar radiation divided by incoming solar radiation at every model step. K_g represents the fraction of incoming solar radiation that needs to be reduced to balance CO_2 forcing. In the GEO simulation, K_g is calculated according to eq. (1) at every model step starting at the implementation of sunshade geoengineering (year 2020), and then solar irradiance is correspondingly reduced by multiplying the value of $1-K_g$ at each grid cell. Using this technique, in the GEO simulation we ensure that reduced solar radiation at global mean base offsets CO_2 radiative forcing at each time step (Figure 1b).

3. Result

3.1 UVic-simulated present day global carbon cycle

UVic-simulated atmospheric CO_2, and oceanic and terrestrial CO_2 uptake during the historical period compares well with data-based estimates as reported by the IPCC fifth assessment report (Ciais et al., 2013; Table 1). For example, data-based estimates show that since preindustrial time, land and ocean have respectively stored 160±90 and 155±30 Pg C of anthropogenic CO_2 emissions, including emissions from fossil fuel combustion, the production of cement, and land use (Ciais et al., 2013). For comparison, during the same time period in the UVic model, simulated land and ocean cumulative CO_2 uptake is 154 and 153 Pg C, respectively. UVic-simulated atmospheric CO_2 also compares well with observations. For example, UVic-simulated annual mean atmospheric CO_2 concentration at year 2010 is 390 ppm (Figure 1c), compared with observed value of 388 ppm (Tans, www.esrl.noaa.gov/gmd/ccgg/trends/). Averaged over the period of 2002–2011, UVic-simulated rate of increasing in atmospheric CO_2 is 4.1 Pg C yr^{-1}, which compares well with the data-based estimate of 4.3±0.2 Pg C yr^{-1} during the same period (Table 1). In addition, the UVic model captures the observed large-scale distribution of carbon-related tracers in different basins of the global ocean, such as dissolved inorganic carbon and alkalinity (refer to supplementary material of Cao et al., 2014).

3.2 Response of carbon cycle

To evaluate the impacts of solar geoengineering, we compare the UVic-simulated Earth system evolution in the A2 and GEO simulations with a focus on the global carbon cycle. Solar geoengineering stabilizes many aspects of CO_2-induced climate change, including temperature, precipitation, sea ice, and large-scale ocean meridional circulation (Appendix Figures A2–A4). A detailed discussion of our results for the physical climate fields can be found in the Appendix.

In our simulations, solar insolation is reduced to balance CO_2 radiative forcing. However, increasing atmospheric CO_2 also causes changes in the growth and distribution of vegetation, which in turn have feedbacks on global climate (Bala et al., 2006). This direct effect of increasing atmospheric CO_2 on global vegetation is not offset by reduced solar insolation. Therefore, in the GEO simulation, there is a small land

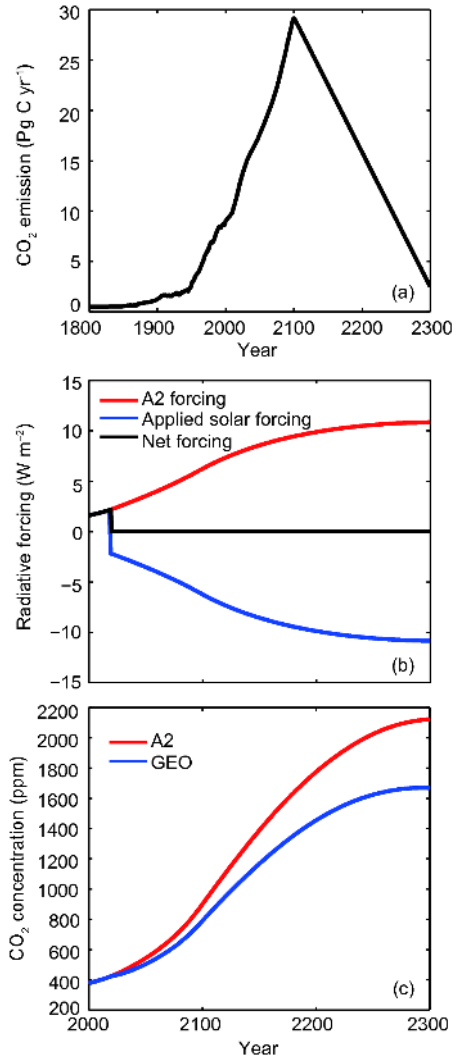

Figure 1 Time series of (a) prescribed CO_2 emission scenario, (b) radiative forcing caused by CO_2 emission (red line), applied negative solar radiative forcing to offset CO_2 radiative forcing (blue line) and net radiative forcing (CO_2+solar) in the GEO simulation (black line), (c) model-simulated atmospheric CO_2 concentration for A2 (red) and GEO (blue) simulations. Solar geoengineering starts at year 2020.

surface warming (0.47 and 0.64 K by year 2100 and 2300, respectively) associated with CO_2-induced expansion of vegetation and resulting decrease in surface albedo (Appendix Figures A5 and A6). This residual land warming will have some effects on the land carbon cycle, but this effect is much smaller than the effect from CO_2 radiative warming.

3.2.1 *Response of the terrestrial carbon cycle*

The key carbon cycle variable values at year 2100 and 2300 are shown in Table 2. In the A2 simulation, increasing atmospheric CO_2 increases land net primary production (NPP, defined as the difference between gross primray production, GPP, and plant respiraiton) primarily as a result of increased photosynthesis via the CO_2 fertilization effect (Owensby et al., 1999). In the A2 simulation, land NPP increases with time but the rate of NPP increase declines with time (Figure 2a), indicating saturation of the CO_2 fertilization effect. Concurrently, soil respiration increases during the simulation period (Figure 2a). Before year ~2120, increasing soil respiration in A2 is caused by increasing temperature, soil moisture and soil carbon storage (Appendix Figure A7). After year ~2120, the effect of increasing temperature and moisture exceeds that of decreased soil carbon storage and thus soil respiration still increases but at a smaller rate (Figure 2a and Appendix Figure A7). Net carbon uptake by the terrestrial biosphere is determined by the difference between NPP and soil respiration. In our A2 simulation, at year 2125, soil respiration exceeds NPP (Figure 2a and 2b), indicating that the global land as a whole turns from a net CO_2 sink to a net CO_2 source. Notably, there are some areas in the northern latitudes that act as CO_2 sink, but the CO_2 sink is counteracted by CO_2 source from large areas in the tropics, as shown in Appendix Figure A8.

Because CO_2-induced warming is largely offset in the GEO simulation (acknowledging the small land-warming associated with CO_2-induced vegetation change as discussed previously), the globally integrated land NPP in the GEO simulation is larger than that of the A2 simulation (Figure 2a) mainly as a result of NPP increase in the tropics (Figure 3c). In the northern middle and high latitudes, land NPP in the GEO simulation is lower than that of A2 because of reduced temperature in the GEO simulation, which suppresses GPP. However, in the tropics, land NPP in the GEO simulation is higher than that of A2 throughout the simulation (Figure 3c, Appendix Figure A9). Before year 2100, higher tropical NPP in GEO than that of A2 is primarily the result of warming-induced increase in plant respiration rate in the A2 simulation. After year 2100, the tropical land area with temperature

Table 1 UVic-simulated global carbon budget compared with data-based estimates[a)]

	Preindustrial–2011 (Pg C)		1980–1989 (Pg C yr^{-1})		1990–1999 (Pg C yr^{-1})		2000–2009 (Pg C yr^{-1})		2002–2011 (Pg C yr^{-1})	
	Data-based estimate	UVic	Data-based estimate	UVic	Data-based estimate	UVic	Data-based estimate	UVic	Data-based estimate	UVic
Atmosphere	240±10	239.3	3.4±0.2	3.2	3.1±0.2	3.3	4.0±0.2	3.8	4.3±0.2	4.1
Land	160±90	153.9	1.5±1.1	2.0	2.6±1.2	2.3	2.6±1.2	2.4	2.5±1.3	2.5
Ocean	155±30	153.1	2.0±0.7	1.8	2.2±0.7	2.1	2.3±0.7	2.4	2.4±0.7	2.5

a) Atmosphere CO_2 increase; Land, CO_2 uptake; Ocean, CO_2 uptake (Ciais et al., 2013)

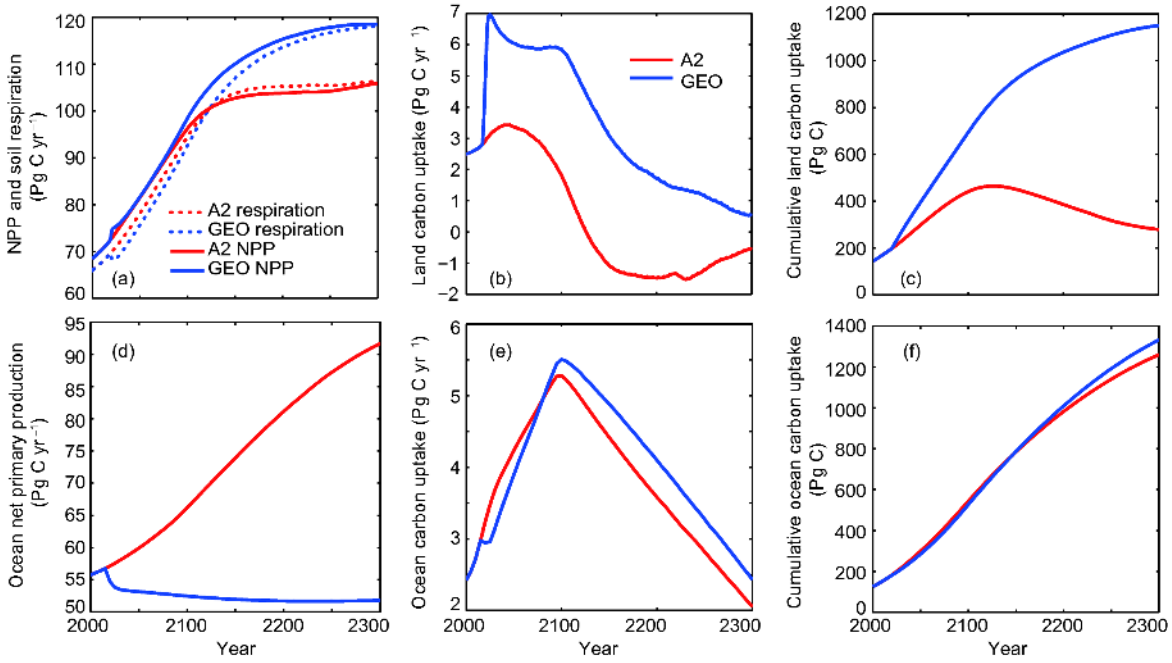

Figure 2 Model-simulated time series of carbon cycle variables for (a) land net primary production (NPP) (solid lines) and soil respiration (dotted lines), (b) annual mean land CO_2 uptake, which is the difference between net primary production and soil respiration (c) cumulative land CO_2 uptake, (d) ocean net primary production, (e) annual mean ocean CO_2 uptake, (f) cumulative ocean CO_2 uptake. Red lines are for the A2 simulation, and blue lines are for the GEO simulation.

Table 2 UVic-simulated change of key carbon cycle variables under the A2 and GEO simulations at year 2100 and 2300 relative to the preindustrial state

Carbon cycle fields	A2		GEO	
	2100	2300	2100	2300
Atmospheric CO_2 (ppm)	900	2123	790	1669
ΔOcean storage (Pg C)	543	1260	526	1332
ΔLand storage (Pg C)	427	258	678	1128
ΔSoil carbon (Pg C)	242	74	476	805
ΔVegetation carbon (Pg C)	185	184	202	323
ΔLand net primary production (Pg C yr^{-1})	40.23	49.12	42.82	61.69
ΔOcean net primary production (Pg C yr^{-1})	13.55	36.03	–0.17	–0.85

higher than 33°C (optimal temperature for photosynthesis of broadleaf tree and shrubs in the tropics in the model. Cox, 2001) gradually expands in the A2 simulation (Appendix Figure A10), which would suppress plant photosynthesis. Therefore, after year 2100, higher tropical NPP in GEO than that of A2 is a result of suppressed plant photosynthesis and increased plant respiration due to increasing temperature in the A2 simulation.

Throughout the simulation period, globally integrated NPP in the GEO simulation is larger than that of A2, which results in a greater amount of carbon in the terrestrial biosphere and soil. Soil respiration is determined by the temperature-dependent rate of respiration, amount of soil carbon storage and soil moisture concentration (Cox, 2001). Before year 2100, global soil respiration in GEO is smaller than that of A2, which is mainly associated with the reduced rate of soil respiration caused by lower temperature in GEO (Appendix Figure A7a). After year 2100, soil respiration in GEO is larger than that of A2 due to higher soil moisture and larger amounts of soil carbon (Figures 2a, Appendix Figure A7b and A7c). Throughout the simulation, net carbon uptake by the terrestrial biosphere (i.e., NPP minus soil respiration) in GEO is larger than that of A2, causing more carbon storage on land and less atmospheric carbon storage (Figures 1c, 3f and 4).

3.2.2 *Response of the ocean carbon cycle*

With increasing of atmospheric CO_2, air-to-sea CO_2 flux in the A2 simulation increases to a peak value of 5.2 Pg C yr^{-1} at year 2100 and decreases to 2.1 Pg C yr^{-1} at year 2300 (Figure 2e). For the GEO simulation, before year 2080, the air-to-sea CO_2 flux is smaller than that of A2 which is mainly

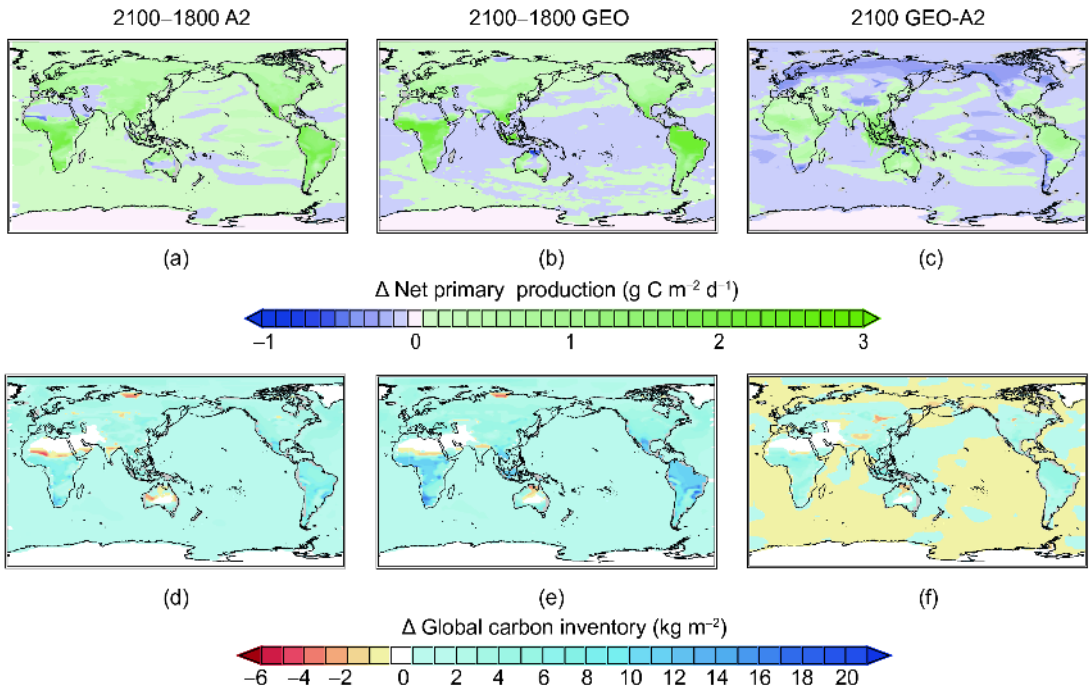

Figure 3 Model-simulated spatial pattern of changes (relative to preindustrial time) in net primary production ((a)–(c)) and carbon inventory ((d)–(f)) for the A2 and GEO simulations at year 2100 and the difference between GEO and A2 at year 2100.

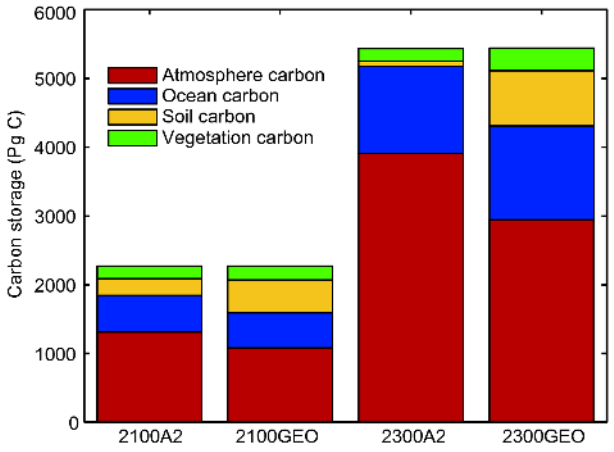

Figure 4 Model-simulated carbon storage in atmosphere, ocean, soil and vegetation at year 2100 and 2300 for the A2 and GEO simulations.

a result of smaller atmospheric CO_2 concentrations in GEO. After year 2080, simulated oceanic CO_2 uptake in GEO becomes larger than that of A2. In the A2 simulation, increased sea surface temperature reduces oceanic CO_2 by decreasing CO_2 solubility. In addition, reduced NADW decreases oceanic uptake of anthropogenic CO_2. In the GEO simulation, both changes in sea surface temperature and NADW are rather small, suppressing the climate effect on oceanic CO_2 uptake. Therefore, as the amount of global warming increases in A2, GEO simulates a larger oceanic CO_2 uptake despite smaller amount of atmospheric CO_2. In our simulations, the total amount of carbon stored in the oceans of GEO exceeds that of A2 after year 2150 (Figure 2f). By year 2300, 6% (72 Pg C) more anthropogenic carbon is sequestered in the ocean for the GEO simulation than that of A2.

In the GEO simulation, due to increased land and ocean carbon uptake compared to that in the A2 simulation, model-simulated atmospheric CO_2 concentration is 12% (110 ppm) and 21% (454 ppm) smaller than that of A2 at year 2100 and 2300, respectively (Figure 1c).

3.3 Response of ocean biogeochemical cycles

In the UVic model, the rate of detritus remineralization depends on temperature (Schmittner et al., 2008), and therefore a warmer ocean leads to a greater rate of organic matter remineralization, producing more nutrients in the upper ocean and thus increasing ocean NPP. In the A2 simulation, relative to the preindustrial level, globally integrated marine NPP increases by 24% and 75% by year 2100 and 2300, respectively (Figure 2d). Throughout the GEO simulation, as a result of the small change in ocean surface temperature, ocean NPP shows small changes relative to the preindustrial value of 52 Pg C yr^{-1}.

In the A2 simulation, global mean ocean oxygen concentration gradually decreases over time primarily as a result of increasing surface temperature that decreases oxygen solubility. By year 2100, in the A2 simulation, the global ocean mean concentration of dissolved oxygen decreases by 5% (Figure 5a), which is within the predicted declining range of 4% to 7% shown in previous studies (Plattner et al., 2001;

Bopp et al., 2001; Matear and Hirst, 2003). By year 2300, simulated global mean ocean oxygen concentration decreases by 14% in the A2 simulation (Figure 5a). The maximum decrease of about 30% in dissolved oxygen is observed at a depth of about 500 m around 40°N (Figure 5b). In the A2 simulation, the suboxic zone (ocean areas where the concentration of dissolved oxygen is less than 10 μmol L^{-1}, Keller et al., 2014) is 1.96×10^7 km^3 (1.5% of the global ocean) at year 2100, which expands to 2.51×10^7 km^3 (1.9% of the global ocean) by year 2300. For comparison, under the GEO simulation, ocean oxygen concentration changes slightly relative to the preindustrial state (Figure 5a and 5c). Also , the size of the suboxic regions in the GEO simulation maintains the preindustrial level of 1.57×10^7 km^3 (1.2% of the global ocean).

4. Discussion and conclusions

Most previous studies of solar geoengineering prescribed atmospheric CO_2 concentration, and therefore neglected the response of the global carbon cycle and its feedback on global climate. Here we conduct solar geoengineering simulations with prescribed CO_2 emissions and analyze the response of the global carbon cycle. Global carbon cycle regulates the amount of atmospheric CO_2 that in turn affects global climate. Therefore, to fully assess the climate response to solar geoengineering, it is important to understand the carbon cycle response to solar geoengineering. In this study, we focus on the carbon cycle response to solar geoengineering. In future study, we will quantify the effect of the carbon cycle feedback on physical climate.

In our simulations, solar geoengineering has a profound effect on the land and ocean carbon cycles. Compared to the A2 scenario without geoengineering, solar geoengineering substantially increases CO_2 uptake by the terrestrial biosphere for two main reasons: (1) reduced temperature acts to increase tropical NPP because warming in the A2 suppresses tropical NPP; (2) reduced temperature reduces the rate of soil respiration. In comparison, solar geoengineering prevents ocean warming and the reduction in large-scale ocean meridional circulation, which cause the ocean to absorb more CO_2 compared to the world without geoengineering. Increased CO_2 uptake by both the land and ocean leads to a lower atmospheric CO_2 content in the solar geoengineering simulation relative to the A2 simulation without geoengineering.

Only a few studies have analyzed the global carbon cycle response to solar geoengineering. Tjiputra et al. (2016), using a comprehensive Earth system model, investigated the response of the land and ocean carbon cycles to solar geoengineering by applying stratospheric aerosol injection (SAI) under RCP 8.5 CO_2 emission scenario. Although our study cannot be directly compared with Tjiputra et al. (2016) due to different solar geoengineering methods and CO_2 emission scenarios, some useful insight can be gained by the comparison between these two studies. Tjiputra et al. (2016) projected cumulative land carbon sinks of 288 Pg C with SAI for year 2020–2100, which is much smaller than that of 478 Pg C simulated in our GEO simulation during the same time period. One reason for this difference is that in their solar geoengineering simulations, there is a residual global warming over preindustrial of about 2 K by year 2100, whereas in our GEO simulation, global mean temperature change by year 2100 is only 0.26 K. A warmer world tends to reduce CO_2 uptake by land through reduced tropical land NPP and/or increased soil respiration (Matthews et al., 2007; Keller et al., 2014). Second, the terrestrial carbon cycle component of Tjiputra et al. (2016) includes the nitrogen limitation, which could substantially suppress simulated land carbon uptake. The smaller land CO_2 sink results in higher atmospheric CO_2 concentration in Tjiputra et al. (2016). By year 2100, their simulated atmospheric CO_2 concentration under SAI is 1084 ppm, while in our GEO simulation atmospheric CO_2 concentration is 790 ppm. For the response of the ocean carbon cycle to SAI, Tjiputra et al. (2016) simulated a cumulative ocean CO_2 sink of 487 Pg C between year 2020 and 2100. During the same period, UVic-modeled ocean carbon storage in the GEO simulation is 326 Pg C. The larger ocean carbon uptake in Tjiputra et al. (2016) can be largely attributed to the higher atmospheric CO_2 concentration as previously discussed. This comparison highlights the importance of coupled land-ocean carbon cycle response to solar geoengineering.

Our results also demonstrate that solar geoengineering has important effects on the ocean biogeochemistry. In our simulation, solar geoengineering, by stabilizing ocean temperature, prevents reduced dissolved oxygen in the ocean and the extension of the suboxic zone. Furthermore, solar geoengineering decreases ocean net primary production as a result of decreased temperature.

The atmosphere component of the UVic model is represented by an energy-moisture balance module that has a simple representation of atmospheric radiation. The lack of explicit representation of direct and diffuse radiation could have important implication for the response of the terrestrial carbon cycle to some solar geoengineering schemes. For example, if solar geoengineering is implemented through stratospheric aerosol injection, diffuse radiation reaching the Earth surface would be increased as a result of increased aerosol concentrations in the stratosphere (Kalidindi et al., 2015). The increased diffuse radiation may increase land NPP and affect land carbon uptake (Mercado et al., 2009; Kalidindi et al., 2015). A detailed investigation of this effect requires a land carbon cycle model that separates the effect of direct and diffuse radiation on terrestrial ecosystem (Mer-

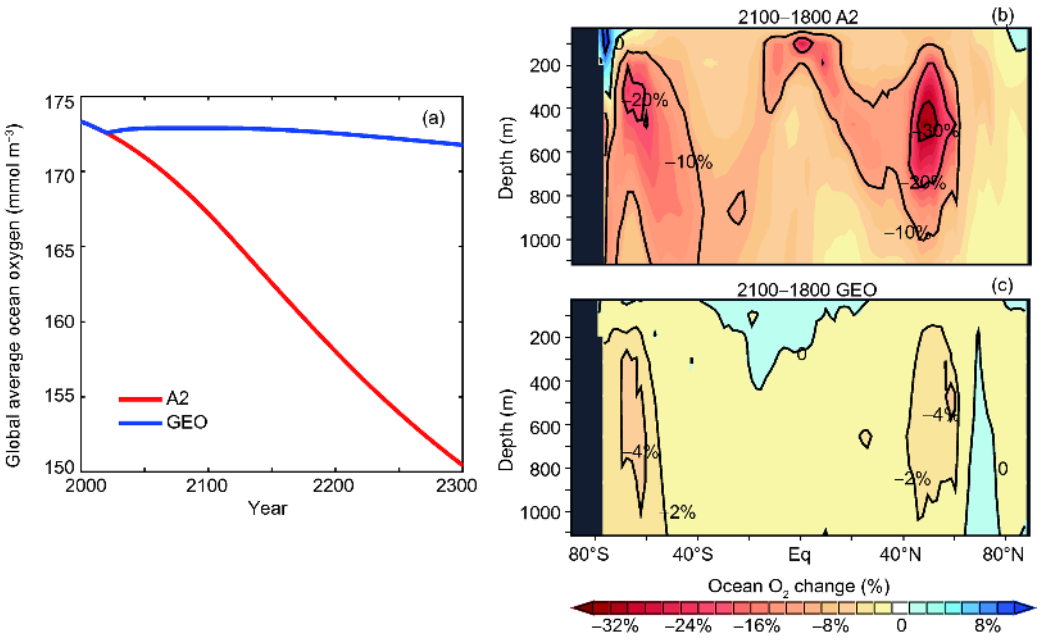

Figure 5 Model-simulated time series of global mean ocean oxygen concentration (a), and latitude-depth distribution of changes (relative to preindustrial state) in ocean dissolved oxygen concentration in the A2 (b) and GEO (c) simulations.

cado et al., 2009), which is beyond the scope of this study.

Furthermore, the land module used in our simulations does not consider nitrogen limitation. Although the mechanisms of nitrogen limitation on biosphere carbon accumulation remain unclear, soil nitrogen would potentially restrict the magnitude of the CO_2 fertilization effect on terrestrial ecosystems in a CO_2-enriched world (Oren et al., 2001; Reich et al., 2006). Therefore, the lack of nitrogen limitation in the land component may overestimate model-simulated NPP of terrestrial vegetation associated with the CO_2 fertilization effect. For example, in Tjiputra et al. (2016), a nitrogen cycle is included in the terrestrial carbon cycle, which partly contributes to a smaller land carbon sink in their geoengineering simulations.

Another uncertainty related to the land carbon cycle response is the response of dynamic vegetation. There are only five plant function types (PFTs) represented in the TRIFFID dynamic vegetation model used in UVic. Models with representation of more PFTs might yield a different terrestrial vegetation response to climate change (Cramer et al., 2001; Sitch et al., 2008). Furthermore, the parameterization schemes in TRIFFID that determine physiological, biophysical, and biogeochemistry processes of terrestrial biosphere are less complicated than some dynamic vegetation models (for example, IBIS), which could generate potential parameter-based uncertainties in the land carbon cycle to climate change and solar geoengineering (Cramer et al., 2001; Sitch et al., 2008).

In terms of the ocean carbon cycle, the representation of marine biology in the UVic model is relatively simple, and hence may neglect potentially important responses of marine biological processes to solar geoengineering, which might affect the simulated ocean carbon cycle. Uncertainties also exist regarding the response of ocean circulation to solar geoengineering and carbon transportation from the surface ocean to deep ocean, which would also affect the response of the ocean carbon cycle.

There are considerable uncertainties about the climate system and global carbon cycle response to solar geoengineering. In addition to the uncertainties related to the climate system response to solar geoengineering, when considering the feasibility of implementing solar geoengineering proposals in the real world, challenges would arise from technology, cost, and risks of solar geoengineering (Matthews and Caldeira, 2007; The Royal Society, 2009; Kravitz et al., 2016). With increasing global temperature as a result of continued greenhouse gas emissions, solar geoengineering might be used as a potential means to mitigate global warming. Therefore, further studies are needed to better understand the consequences and risks of solar geoengineering.

Here we conduct highly idealized sunshade geoengineering simulations using an Earth system model of intermediate complexity; more studies using comprehensive climate-carbon cycle models are needed to further investigate the interactions between the carbon cycle and solar geoengineering. Ongoing GeoMIP studies simulate climate response to different solar geoengineering schemes under prescribed atmospheric CO_2 concentration (Kravitz et al., 2015). Similar multi-model simulations on solar geoengineering that consider an interactive carbon cycle are encouraged to obtain a more reliable projection of climate

change and the global carbon cycle response to solar geoengineering.

Acknowledgements *Dataset used for results reported in the paper and model source code for each simulation experiment are deposited at the supercomputer center at Zhejiang University and can be obtained by contacting longcao@zju.edu.cn. This work was supported by the National Key Basic Research Program of China (Grant No. 2015CB953601), the National Natural Science Foundation of China (Grant Nos. 41675063 & 41422503), and the Fundamental Research Funds for the Central Universities.*

References

Bala G, Caldeira K, Mirin A, Wickett M, Delire C, Phillips T J. 2006. Biogeophysical effects of CO_2 fertilization on global climate. Tellus B-Chem Phys Meteorol, 58: 620–627

Boden T A, Marland G, Andres R J. 2016. Global, regional, and national fossil-fuel CO_2 emissions. Carbon Dioxide Information Analysis Center, Oak Ridge National Laboratory, US Department of Energy, Oak Ridge

Bopp L, Monfray P, Aumont O, Dufresne J L, Le Treut H, Madec G, Terray L, Orr J C. 2001. Potential impact of climate change on marine export production. Glob Biogeochem Cycle, 15: 81–99

Brovkin V, Petoukhov V, Claussen M, Bauer E, Archer D, Jaeger C. 2009. Geoengineering climate by stratospheric sulfur injections: Earth system vulnerability to technological failure. Clim Change, 92: 243–259

Caldeira K, Bala G, Cao L. 2013. The science of geoengineering. Annu Rev Earth Planet Sci, 41: 231–256

Cao L, Duan L, Bala G, Caldeira K. 2016. Simulated long-term climate response to idealized solar geoengineering. Geophys Res Lett, 43: 2209–2217

Cao L, Wang S, Zheng M, Zhang H. 2014. Sensitivity of ocean acidification and oxygen to the uncertainty in climate change. Environ Res Lett, 9: 064005

Ciais P, Sabine C, Bala G, Bopp L, Brovkin V, Canadell J, Chhabra A, DeFries R, Galloway J, Heimann M, Jones C, Le Quéré C, Myneni R B, Piao S, Thornton P. 2013. Carbon and other biogeochemical cycles. In: Stoker T F, Qin D, Plattner G K, Tignor M, Allen S K, Boschung J, Nauels A, Xia Y, Bex V, Midgley P M, eds. Climate Change 2013. The physical science basis. Contribution of Working Group I to the Fifth Assessment Report of the Intergovernmental Panel on Climate Change. Cambridge: Cambridge University Press. 465–570

Cox P M. 2001. Description of the TRIFFID dynamic global vegetation model. Hadley Centre Technical Note. 24: 1–16

Cramer W, Bondeau A, Woodward F I, Prentice I C, Betts R A, Brovkin V, Cox P M, Fisher V, Foley J A, Friend A D, Kucharik C, Lomas M R, Ramankutty N, Sitch S, Smith B, White A, Young-Molling C. 2001. Global response of terrestrial ecosystem structure and function to CO_2 and climate change: Results from six dynamic global vegetation models. Glob Change Biol, 7: 357–373

Crutzen P J. 2006. Albedo enhancement by stratospheric sulfur injections: A contribution to resolve a policy dilemma? Clim Change, 77: 211–220

Curry C L, Sillmann J, Bronaugh D, Alterskjaer K, Cole J N S, Ji D, Kravitz B, Kristjánsson J E, Moore J C, Muri H, Niemeier U, Robock A, Tilmes S, Yang S. 2014. A multimodel examination of climate extremes in an idealized geoengineering experiment. J Geophys Res-Atmos, 119: 3900–3923

Early J T. 1989. Space-based solar shield to offset greenhouse effect. J Brit Interplanet Soc, 42: 567–569

Eby M, Zickfeld K, Montenegro A, Archer D, Meissner K J, Weaver A J. 2009. Lifetime of anthropogenic climate change: Millennial time scales of potential CO_2 and surface temperature perturbations. J Clim, 22: 2501–2511

Eliseev A V, Chernokulsky A V, Karpenko A A, Mokhov I I. 2010. Global warming mitigation by sulphur loading in the stratosphere: Dependence of required emissions on allowable residual warming rate. Theor Appl Climatol, 101: 67–81

Govindasamy B, Thompson S, Duffy P B, Caldeira K, Delire C. 2002. Impact of geoengineering schemes on the terrestrial biosphere. Geophys Res Lett, 29: 18-1–18-4

Houghton R A, House J I, Pongratz J, van der Werf G R, DeFries R S, Hansen M C, Le Quéré C, Ramankutty N. 2012. Carbon emissions from land use and land-cover change. Biogeosciences, 9: 5125–5142

IPCC. 2001. Climate change 2001. In: Metz B, Davidson O, Swart R, eds. Mitigation: Contribution of Working Group III to the Third Assessment Report of the Intergovernmental Panel on Climate Change. Cambridge: Cambridge University Press. 752

IPCC. 2007. Climate change 2007. In: Solomon S E, ed. The Physical Science Basis. Contribution of Working Group I to the Fourth Assessment Report of the Intergovernmental Panel on Climate Change. Cambridge: Cambridge University Press. 996

Irvine P J, Lunt D J, Stone E J, Ridgwell A. 2009. The fate of the Greenland Ice Sheet in a geoengineered, high CO_2 world. Environ Res Lett, 4: 045109

Kalidindi S, Bala G, Modak A, Caldeira K. 2015. Modeling of solar radiation management: A comparison of simulations using reduced solar constant and stratospheric sulphate aerosols. Clim Dyn, 44: 2909–2925

Keith D W. 2000. Geoengineering the climate: History and prospect. Annu Rev Energy Environ, 25: 245–284

Keller D P, Feng E Y, Oschlies A. 2014. Potential climate engineering effectiveness and side effects during a high carbon dioxide-emission scenario. Nat Commun, 5: 3304

Kravitz B, Robock A, Boucher O, Schmidt H, Taylor K E, Stenchikov G, Schulz M. 2011. The Geoengineering model intercomparison project (GeoMIP). Atmos Sci Lett, 12: 162–167

Kravitz B, Caldeira K, Boucher O, Robock A, Rasch P J, Alterskjaer K, Karam D B, Cole J N S, Curry C L, Haywood J M, Irvine P J, Ji D, Jones A, Kristjánsson J E, Lunt D J, Moore J C, Niemeier U, Schmidt H, Schulz M, Singh B, Tilmes S, Watanabe S, Yang S, Yoon J H. 2013. Climate model response from the geoengineering model intercomparison project (GeoMIP). J Geophys Res-Atmos, 118: 8320–8332

Kravitz B, Robock A, Tilmes S, Boucher O, English J M, Irvine P J, Jones A, Lawrence M G, MacCracken M, Muri H, Moore J C, Niemeier U, Phipps S J, Sillmann J, Storelvmo T, Wang H, Watanabe S. 2015. The geoengineering model intercomparison project phase 6 (GeoMIP6): Simulation design and preliminary results. Geosci Model Dev, 8: 3379–3392

Kravitz B, MacMartin D G, Wang H, Rasch P J. 2016. Geoengineering as a design problem. Earth Syst Dynam, 7: 469–497

Kvenvolden K A. 2002. Methane hydrate in the global organic carbon cycle. Terra Nova, 14: 302–306

Lunt D J, Ridgwell A, Valdes P J, Seale A. 2008. "Sunshade World": A fully coupled GCM evaluation of the climatic impacts of geoengineering. Geophys Res Lett, 35: L12710

Matear R J, Hirst A C. 2003. Long-term changes in dissolved oxygen concentrations in the ocean caused by protracted global warming. Glob Biogeochem Cycle, 17: 1125

Matthews H D, Caldeira K. 2007. Transient climate carbon simulations of planetary geoengineering. Proc Natl Acad Sci USA, 104: 9949–9954

Matthews H D, Eby M, Ewen T, Friedlingstein P, Hawkins B J. 2007. What determines the magnitude of carbon cycle-climate feedbacks? Glob Biogeochem Cycle, 21: GB2012

Meissner K J, Weaver A J, Matthews H D, Cox P M. 2003. The role of land surface dynamics in glacial inception: A study with the UVic Earth System Model. Clim Dyn, 21: 515–537

Mercado L M, Bellouin N, Sitch S, Boucher O, Huntingford C, Wild M, Cox P M. 2009. Impact of changes in diffuse radiation on the global land carbon sink. Nature, 458: 1014–1017

National Research Council. 2015a. Climate Intervention: Carbon Dioxide Removal and Reliable Sequestration. Washington D C: The National Academies Press. 154

National Research Council. 2015b. Climate Intervention: Reflecting Sun-

light to Cool Earth. Washington D C: The National Academies Press. 260
Niemeier U, Schmidt H, Alterskjaer K, Kristjánsson J E. 2013. Solar irradiance reduction via climate engineering: Impact of different techniques on the energy balance and the hydrological cycle. J Geophys Res-Atmos, 118: 11905–11917
Oren R, Ellsworth D S, Johnsen K H, Phillips N, Ewers B E, Maier C, Schäfer K V R, McCarthy H, Hendrey G, McNulty S G, Katul G G. 2001. Soil fertility limits carbon sequestration by forest ecosystems in a CO_2-enriched atmosphere.. Nature, 411: 469–472
Orr J, Najjar R, Sabine C, Joos F. 1999. Abiotic-HOWTO, internal OCMIP report. LSCE/CEA Saclay, 25
Owensby C E, Ham J M, Knapp A K, Auen L M. 1999. Biomass production and species composition change in a tallgrass prairie ecosystem after long-term exposure to elevated atmospheric CO_2. Glob Change Biol, 5: 497–506
Plattner G K, Joos F, Stocker T F, Marchal O. 2001. Feedback mechanisms and sensitivities of ocean carbon uptake under global warming. Tellus B, 53: 564–592
Rasch P J, Tilmes S, Turco R P, Robock A, Oman L, Chen C C, Stenchikov G L, Garcia R R. 2008. An overview of geoengineering of climate using stratospheric sulphate aerosols. Philos Trans R Soc A-Math Phys Eng Sci, 366: 4007–4037
Reich P B, Hobbie S E, Lee T, Ellsworth D S, West J B, Tilman D, Knops J M H, Naeem S, Trost J. 2006. Nitrogen limitation constrains sustainability of ecosystem response to CO_2. Nature, 440: 922–925
Ridgwell A, Singarayer J S, Hetherington A M, Valdes P J. 2009. Tackling regional climate change by leaf albedo bio-geoengineering. Curr Biol, 19: 146–150
Robock A. 2014. Stratospheric aerosol geoengineering. Issues Environ Sci Technol, 38: 162–185
Salter S, Sortino G, Latham J. 2008. Sea-going hardware for the cloud albedo method of reversing global warming. Philos Trans R Soc A-Math Phys Eng Sci, 366: 3989–4006
Schmittner A, Oschlies A, Matthews H D, Galbraith E D. 2008. Future changes in climate, ocean circulation, ecosystems, and biogeochemical cycling simulated for a business-as-usual CO_2 emission scenario until year 4000 AD. Glob Biogeochem Cycle, 22: GB1013
Sitch S, Huntingford C, Gedney N, Levy P E, Lomas M, Piao S L, Betts R, Ciais P, Cox P, Friedlingstein P, Jones C D, Prentice I C, Woodward F I. 2008. Evaluation of the terrestrial carbon cycle, future plant geography and climate-carbon cycle feedbacks using five dynamic global vegetation models (DGVMs). Glob Change Biol, 14: 2015–2039
The Royal Society. 2009. Geoengineering the Climate: Science, Governance and Uncertainty. London: Royal Society
Tilmes S, Fasullo J, Lamarque J F, Marsh D R, Mills M, Alterskjaer K, Muri H, Kristjánsson J E, Boucher O, Schulz M, Cole J N S, Curry C L, Jones A, Haywood J, Irvine P J, Ji D, Moore J C, Karam D B, Kravitz B, Rasch P J, Singh B, Yoon J H, Niemeier U, Schmidt H, Robock A, Yang S, Watanabe S. 2013. The hydrological impact of geoengineering in the geoengineering model intercomparison project (GeoMIP). J Geophys Res-Atmos, 118: 11036–11058
Tjiputra J F, Grini A, Lee H. 2016. Impact of idealized future stratospheric aerosol injection on the large-scale ocean and land carbon cycles. J Geophys Res-Biogeosci, 121: 2–27
Trenberth K E, Fasullo J T, Kiehl J. 2009. Earth's global energy budget. Bull Amer Meteorol Soc, 90: 311–324
Vaughan N E, Lenton T M. 2011. A review of climate geoengineering proposals. Clim Change, 109: 745–790
Victor D G, Zhou D, Ahmed E H M, Dadhich P K, Olivier J G J, Rogner H H, Sheikho K, Yamaguchi M. 2014. Climate Change 2014: Mitigation of Climate Change. In: Edenhofer O, Pichs-Madruga R, Sokona Y, Farahani E, Kadner S, Seyboth K, Adler A, Baum I, Brunner S, Eickemeier P, Kriemann B, Savolainen J, Schlömer S, von Stechow C, Zwickel T, Minx J C, eds. Contribution of Working Group III to the Fifth Assessment Report of the Intergovernmental Panel on Climate Change. Cambridge: Cambridge University Press. 113–143
Weaver A J, Eby M, Wiebe E C, Bitz C M, Duffy P B, Ewen T L, Fanning A F, Holland M M, MacFadyen A, Matthews H D, Meissner K J, Saenko O, Schmittner A, Wang H, Yoshimori M. 2001. The UVic earth system climate model: Model description, climatology, and applications to past, present and future climates. Atmos-Ocean, 39: 361–428

(Responsible editor: Haibin WU)